Flexible and Printed Electronics

A printable GO-PVA composite dielectric for EDL gating of metal-oxide TFTs

Xinchi Wang, Li Wei, Penglin Mou, Feng Shao ⓘ and Xiaofeng Gu

Engineering Research Center of IoT Technology Applications (Ministry of Education), Department of Electronic Engineering, Jiangnan University, Wuxi 214122, People's Republic of China

E-mail: sf@jiangnan.edu.cn

Abstract

Printing fabrication and 2D materials are both intriguing concepts for developing electronic devices and circuits. In this paper, a home-built nozzle jet printing system was used to deposit the graphene oxide-poly(vinyl alcohol) (GO-PVA) composite dielectric for metal-oxide-based thin-film transistors. With further reduction possible, a minimum line width of about 330 μm was demonstrated by using the current setup. The GO-PVA composite dielectric here works as an ion-based dielectric, which modulates the transistor current with an electric-double-layer effect. The obtained device therefore operates in a small gate voltage range of -0.5 to 2.5 V. It was found that the incorporation of PVA into GO was beneficial as it makes the device more stable and testable. Possible reasons that caused the instability of the pure GO-based device were analyzed.

1. Introduction

Electrostatic gating with ion-based dielectrics has been extensively studied under the name of electrolyte-gated, ion-gated or proton-gated transistors [1–3]. In principle, these devices share the same charge modulation mechanism of electric-double-layer (EDL) gating [4]. The formation of the EDL capacitance at the semiconductor-dielectric interface brings high charge carrier density ($>10^{14}$ cm^{-2}) with a typical gate bias of less than 2 V [5, 6]. Along with the low working voltage, this category of newly emerged transistor devices has demonstrated interesting results in chemical sensing, artificial synapse mimicking and multi-gate logic [7–10].

Graphene oxide (GO) is a non-conductive derivative of graphene. It can be easily produced in a large quantity by liquid phase exfoliation of graphite. Its 2D structure provides GO with a large surface area, which is covered by hydrophilic functional groups, such as –O–, –COOH and –OH to a great extent. This makes GO highly dispersible in common polar or nonpolar solvents without the use of any stabilizer [11, 12]. GO therefore has become an important ink component in the development of printed electronics [13, 14].

The adsorption of H_2O and formation of hydrogen bonds on GO then enable proton migration by hopping through the molecular network of hydrogen bonds (the Grotthuss mechanism) [15, 16]. The path of migration might be over the basal plane, around the plane edge or through the pinholes of the 2D sheets [17]. As a result, GO film that is assembled from dispersed GO sheets behaves as an ionic conductor and electric insulator at the same time, allowing it to serve simultaneously as an electrolyte and a dielectric. Accordingly, GO films were investigated as the electrolyte in EDL supercapacitors, proton exchange membrane in fuel cells and more recently as the gate dielectric in proton-gated EDL transistors (EDLTs) [18–20].

Despite the successful demonstration of its functionality, it was also pointed out that the mechanical stability of pure GO film posed an issue [19, 21]. The GO film was found to disintegrate under the stress of gas flow in the fuel cell [19]. The problem of swelling is also severe due to high water uptake ($\sim$16 wt%). The difference in interlayer spacing between the hydrated and dehydrated GO films is about 30% [18]. Therefore, surface modification or adding polymer binder were proposed to enhance the mechanical stability of the GO film [21].
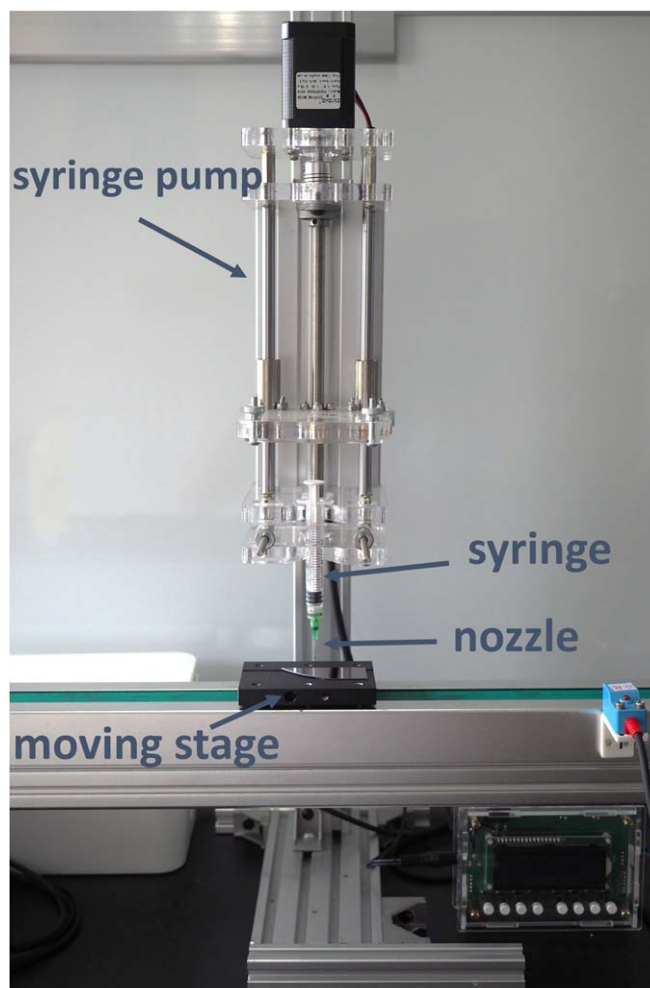
Figure 1. Photo of the home-built nozzle jet printing system.

In this paper, poly(vinyl alcohol) (PVA) was added into the dispersion of GO as a binder to form the GO-PVA composite dielectric ink. Printing deposition of line-shaped GO-PVA composite dielectric ink was realized by using nozzle jet printing. The main advantage of using the nozzle jet printing technique here is its high deposition yield, compatibility with viscous ink and low build cost. The basic properties of the GO-PVA composite dielectric were characterized. The IGZO EDLTs with GO-PVA composite dielectric were fabricated by the nozzle jet printing of GO-PVA dielectric ink and magnetron sputtering of IGZO channel and IZO electrodes. The prepared device showed on/off ratio of 2.3×10^4 and field mobility of $0.06 \ cm^2 \ V^{-1}s^{-1}$ in a small gate voltage range of -0.5 to 2.5 V. It was also found that the device with GO-PVA dielectric showed improved stability compared to that with pure GO. The reason could be ascribed to the poor structural stability of pure GO dielectric and the binder effect of PVA.

2. Experimental

2.1. Ink preparation

To prepare $6 \ mg \ ml^{-1}$ GO-PVA ink solution, 37.8 mg of single-layer GO powder ($0.2 \sim 10 \ \mu m$ sheet diameter, Tanfeng Tech. Inc.) was added into 3 ml of deionized water. It was dispersed by an ultrasonic cell crusher at the power of 350 W for 6 h under external liquid cooling. 3 ml of ethanol and 3 ml of ethylene glycol were further added as co-solvent. 16.2 mg of PVA ($54 \ mPa \cdot s \sim 66 \ mPa \cdot s$ viscosity, Aladdin) was then added and dissolved by stirring in a water bath at $80 \ ^\circ C$. The PVA finally accounted for 30 wt% of the total dry material. The surface tension and viscosity of the GO-PVA ink were measured to be $29.1 \ mN \ m^{-1}$ and $11.5 \ mPa \cdot s$, respectively.

2.2. Nozzle jet printing

A home-built nozzle jet printing system was used to deposit the GO-PVA composite dielectric. As shown in figure 1(a), it consists of a vertical syringe pump, syringe with stainless-steel nozzle and one-directional moving stage. The syringe pump has a downward compression speed of $0.01 \ mm \ s \sim 2 \ mm \ s^{-1}$, which
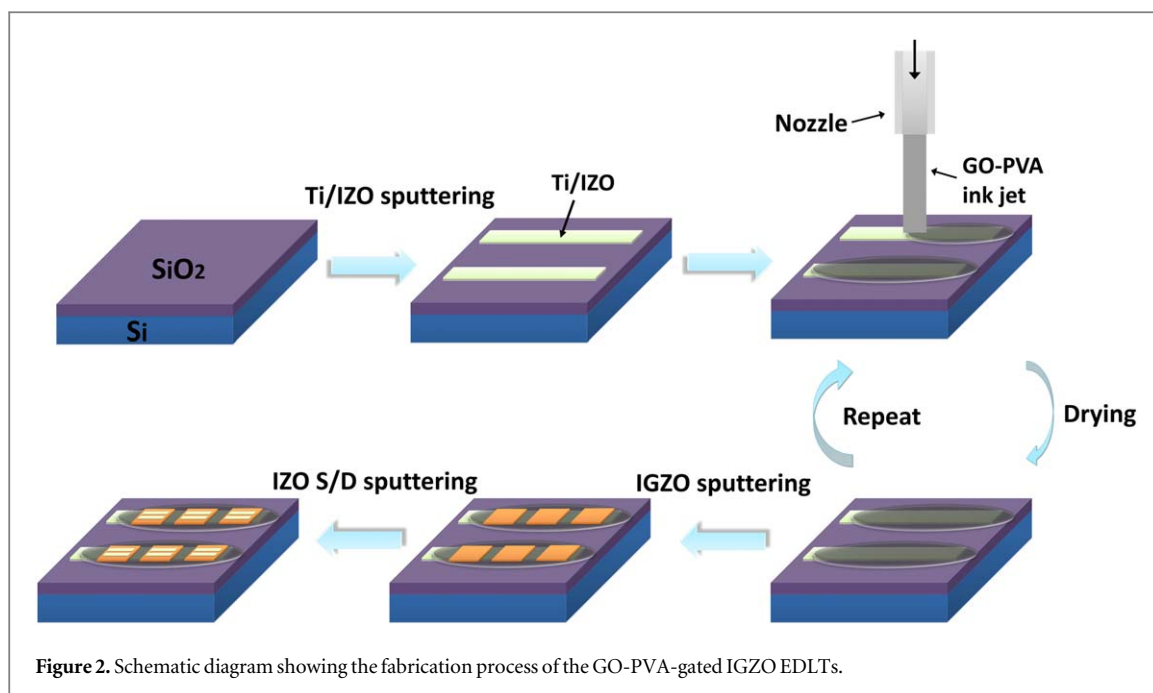
Figure 2. Schematic diagram showing the fabrication process of the GO-PVA-gated IGZO EDLTs.

corresponds to the flow rate of 0.79 ~157 $\mu l\,s^{-1}$ when equipped with a 3 ml syringe. The nozzle used has an inner diameter down to 60 μm. The moving stage has a speed range of 100 mm~1000 mm s^{-1}. The pump compression speed to allow ink jetting was first determined. The minimal printing line width was then demonstrated by ink jetting at increased stage moving velocities.

2.3. Dielectric characterization

For the basic material and electrical characterizations of the GO-PVA dielectric, GO-PVA films were deposited by drop casting 80 $\mu l\,cm^{-2}$ of the prepared GO-PVA ink onto 2.5 × 2.5 cm ITO glass and dried at 80 °C for 3 h in an oven. This process was repeated up to six times to achieve increased dielectric thickness. The film thickness was measured with a profilometer (KLA Tencor D120). IZO electrodes were sputtered on top of the film to have the IZO/GO-PVA/ITO structure for leakage current measurement with a sourcemeter, and for frequency-dependent capacitance measurement with an LCR meter (IM3533-01, Hioki). Fourier transform infrared spectroscopy (FTIR) (IRTracer-100, Shimadzu) spectra were measured by depositing GO-PVA onto silicon substrate. The surface morphology was measured with an atomic force microscope (AFM) (NTEGRA, NT-MDT).
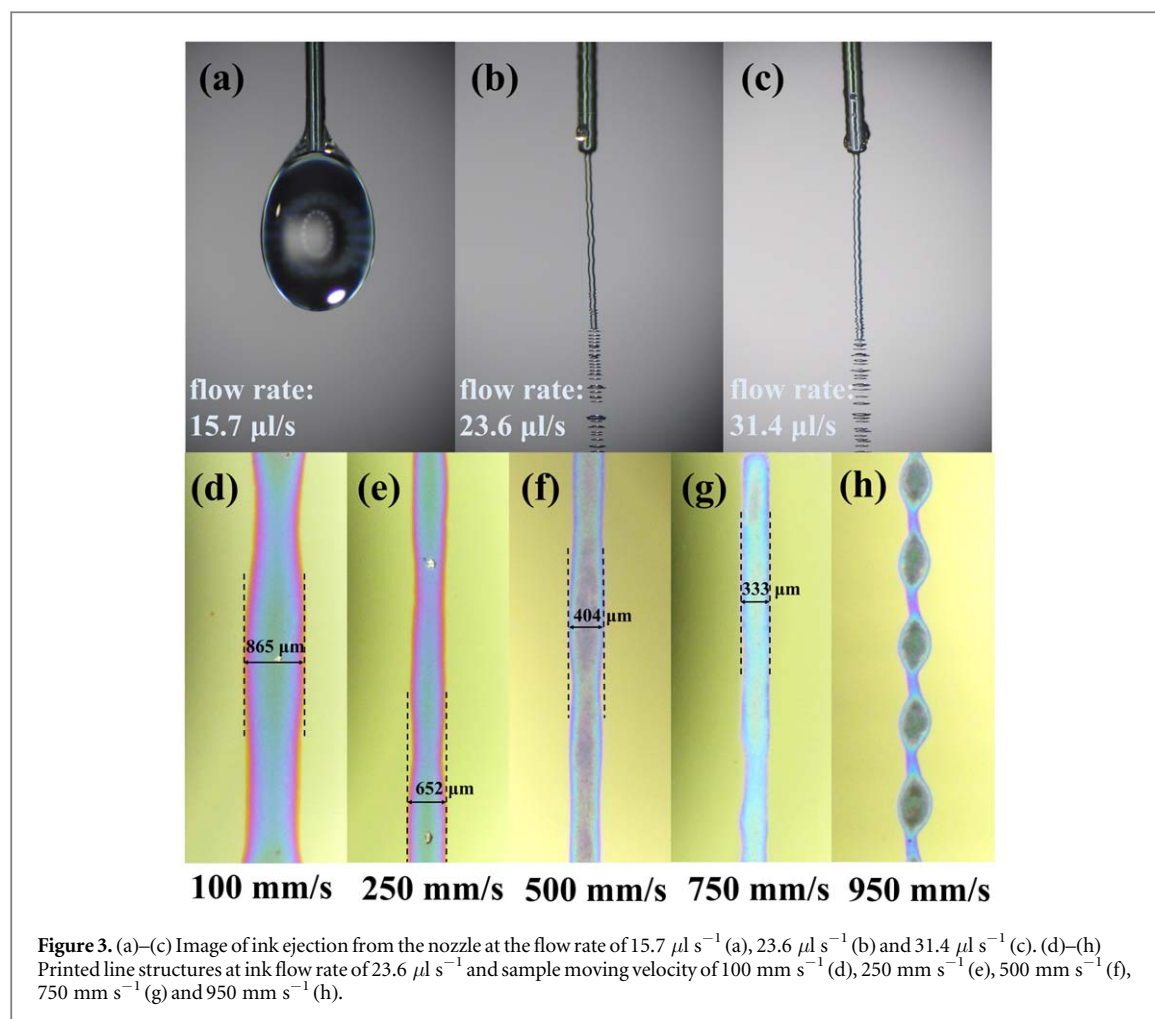
2.4. EDLT fabrication

The oxide-based EDLTs with GO-PVA dielectric were fabricated on Si/SiO$_2$ substrates. As illustrated in figure 2, the long strip of conductive Ti/IZO electrodes were first deposited on the SiO$_2$ surface by DC and RF magnetron sputtering, consecutively. Here, the Ti layer works as an adhesion layer for the IZO bottom gate. GO-PVA was deposited by the nozzle printing

system at the substrate with a moving speed of 500 mm s^{-1}. The printed structure was dried at 80 °C for 3 h. The printing and drying processes were repeated to increase the ink loading and dielectric thickness. An IGZO semiconductor layer about 40 nm thick was then deposited on top of the GO-PVA dielectric by RF magnetron sputtering at room temperature (target In:Ga:Zn:O = 1:1:1:4, atomic ratio). The deposition was performed with Ar gas at the pressure of 0.3 Pa and power of 80 W. The source/drain (S/D) IZO electrodes were then deposited by RF sputtering (Ar, 0.3 Pa, 80 W). Stainless-steel shadow masks were used to define the area of the electrodes and IGZO deposition. The defined semiconductor channel has the width of 1000 and length of 80 μm (*W*: *L* = 12.5). Electrical measurements were performed with a probe station, which was connected to the sourcemeter (2602A, Keithley).

3. Results

3.1. Printability of the nozzle jet printing system

Since ink jetting instead of ink droplet dropping is the basic idea that allows the nozzle jet printing technique to print fine structures controllably, it is necessary to first determine the right ink flow rate (syringe pump compression speed) for the ink to jet. As shown in figures 3(a)–(c), the outcoming ink remained as large droplets at the flow rate of 15.7 $\mu l\,s^{-1}$ (0.2 mm s^{-1}). Ink jetting started at the flow rate of 23.6 $\mu l\,s^{-1}$ (0.3 mm s^{-1}). The ejected ink formed a liquid column that largely retained the inner dimension of the nozzle. The length of the ejected ink column was estimated to be 2.1 mm from the image. Over this length, the ink column started to split into droplets as a result of kinetic energy loss. Further increase of the flow rate to

Figure 3. (a)–(c) Image of ink ejection from the nozzle at the flow rate of 15.7 μl s^{-1} (a), 23.6 μl s^{-1} (b) and 31.4 μl s^{-1} (c). (d)–(h) Printed line structures at ink flow rate of 23.6 μl s^{-1} and sample moving velocity of 100 mm s^{-1} (d), 250 mm s^{-1} (e), 500 mm s^{-1} (f), 750 mm s^{-1} (g) and 950 mm s^{-1} (h).

31.4 μl s^{-1} (0.4 mm s^{-1}) caused a minor increase in ejection length.

Relative velocity of the sample to nozzle is an important parameter that influences the printing outcome. In principle, rapid movement of the nozzle would reduce the amount of ink deposited onto the average surface area and therefore lower the line width of the printed feature. Figures 3(d)–(h) show the printed line structures when the ink flow rate was maintained at 23.6 μl s^{-1} for ink jetting and changing the sample stage moving velocity from 100 up to 950 mm s^{-1}. The line width dropped continuously and the line shape was maintained till the velocity of 750 mm s^{-1}. At 950 mm s^{-1}, the printed line spontaneously turned into interconnected larger drops due to the tendency of lowering the surface energy. The minimum line width of 333 μm obtained here is comparable to other reports on nozzle jet printing [22–24]. The printed line width however is also related to nozzle size, surface wettability, nozzle to sample distance and ink fluidic properties, which can therefore be further adjusted [24, 25].

3.2. Material and electrical properties of the GO-PVA dielectric

To have an electric insulating film of GO-PVA composite, the thickness of the film was increased stepwise by repeating the drop casting and drying process. As shown in figure 4(a), the thickness of the obtained films increased when more ink solution was added. The measured current densities of the IZO/GO-PVA/ITO sandwich structures with different dielectric thicknesses are given in figure 4(b). Overall, the current density dropped as the dielectric thickness increased. The films of 80 and 160 μl cm^{-2} had high current density and the curves showed ohmic behavior as the I/V relation was almost linear and the curve passed through the zero point. These films were therefore determined to be electric non-insulating due to the porosity of the GO-PVA composite dielectric. The curves of thicker dielectrics did not pass through the zero point and showed clear hysteresis, which is typical for ion-based dielectrics and indicates that the current was mainly formed by proton (ion) involved charging and discharging of electrodes [10, 26, 27]. The decrease of the current density in logarithmic scale was caused by the current reversing when charging and discharging switches. The suppressed electric leakage current of the thicker film ensured low gate current of thin-film transistors. The ink density of
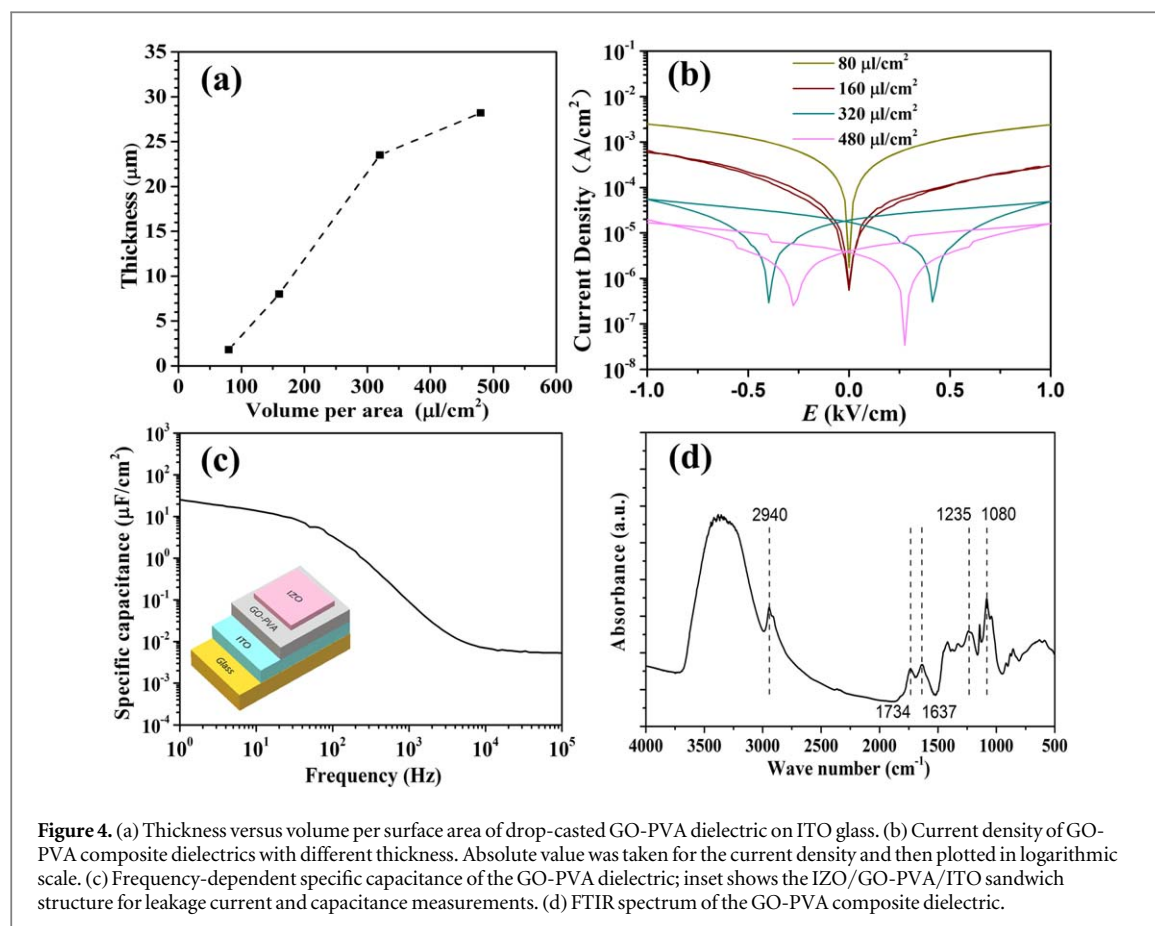
Figure 4. (a) Thickness versus volume per surface area of drop-casted GO-PVA dielectric on ITO glass. (b) Current density of GO-PVA composite dielectrics with different thickness. Absolute value was taken for the current density and then plotted in logarithmic scale. (c) Frequency-dependent specific capacitance of the GO-PVA dielectric; inset shows the IZO/GO-PVA/ITO sandwich structure for leakage current and capacitance measurements. (d) FTIR spectrum of the GO-PVA composite dielectric.

320 μl cm^{-2} was then adopted in the further study. The demand on large ink volume demonstrated here is one of the reasons the nozzle jet printing was used.

Large capacitance at low frequency and strong frequency dependence are both characteristics of EDL capacitance. Figure 4(c) shows the frequency-dependent capacitance of the 320 μl cm^{-2} GO-PVA dielectric. The specific capacitance reached 25 μFcm^{-2} at 1 Hz, which was very close to the value reported for pure GO film [20]. The continuous decrease of specific capacitance over a wide frequency range indicates that the high capacitance at low frequency results from the slow polarization process of ions (protons here) [28–30]. As the frequency increases, EDL capacitance fades due to the slow response of protons, and the dipole polarization of bulk material dominates [31].

Figure 4(d) shows the FTIR spectrum of the GO-PVA dielectric. The C=O stretching vibration in the carboxyl group was observed at 1734 cm^{-1}. The peak for C=C bond was observed at 1637 cm^{-1}. The absorption peak at 1235 cm^{-1} was generated by the C–O–C stretching vibration and the peak at 1080 was from the C–O stretching vibration in the CH–OH group [32]. The peak at 2940 cm^{-1} is characteristic of C–H stretching. The broad band between 3600 and 3000 cm^{-1} is known for the O–H bond of the hydroxyl group and water [33]. The GO-PVA composite dielectric therefore has a large amount of H-containing molecules that can release protons and also assist with their migration.

3.3. EDLT performance

Figures 5(a) and (b) are the transfer and output curves of the IGZO EDLT with nozzle jet printed GO-PVA dielectric. As can be seen, the anti-clockwise hysteresis was observed in the transfer curve due to the slow relaxation of protons at the interface. The device has an on/off ratio of 2.3×10^4 in a small V_{gs} range of -0.5 to 2.5 V. The threshold voltage V_{th} was found at 1 V. The field-effect mobility μ was calculated to be 0.06 cm^2/Vs using equation: $I_{ds} = \left(\frac{\mu WC_i}{2L}\right)(V_{gs} - V_{th})^2$, where C_i is the specific capacitance of the gate dielectric (C_i value at 1 Hz was used), V_{th} is the threshold voltage, and W and L are the width and length of the IGZO channel, respectively. This was addressed by Wang *et al* [34], who found that the use of the quasi-static state C_i is more precise for EDL dominated transistors. Output curves showed linear ohmic contact behavior at low V_{ds} and current saturation at higher V_{ds}. In terms of the device performance uniformity, statistical data of ten devices from the same piece of Si substrate are given in figure S2.

The stability of any newly developed device could be a cause for concern. In practice, we experienced poor test durability on the IGZO EDLTs with pure GO as the gate dielectric. As shown in figures 6(a) and (b),
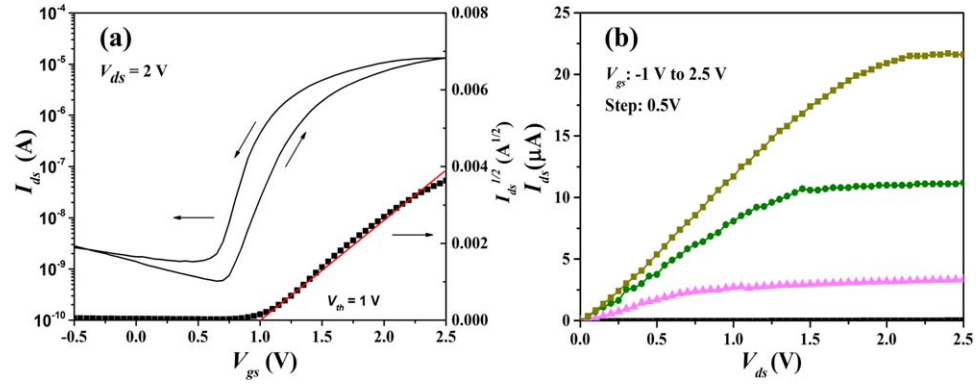
Figure 5. (a) Transfer curve of IGZO EDLT gated by GO-PVA dielectric. (b) Output curves of IGZO EDLT gated by GO-PVA dielectric.
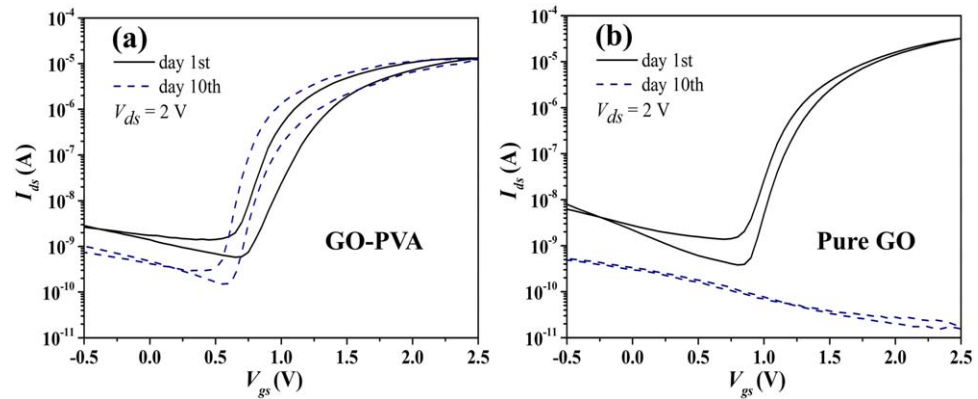

Figure 6. (a) Transfer curves of IGZO EDLT gated by GO-PVA dielectric. (b) Transfer curves of IGZO EDLT gated by GO dielectric.

the test durability was clearly better with the GO-PVA dielectric. After ten days of storage, both devices had a decline in off state I_{ds} and the pure GO-based device completely lost the transfer characteristic. However, for the GO-PVA-based device, ion-based field-effect modulation of the channel current was sustained. The transfer curve was still measurable despite showing a certain degree of drift. Along with the loss of transfer characteristic, it was also noted that the IZO S/D electrodes became significantly less conductive on the pure GO device. The conductivity on the pure GO device was lower by two orders of magnitude compared to that on the GO-PVA device.

As mentioned earlier, the binding between pure GO is weak. Microscale expansion and contraction would be severe when hydration and dehydration take place following the environmental moisture level change. Here, we conclude that such structural instability is causing the failure of the pure GO-based devices. The structural integrity of the IGZO channel and IZO electrodes is subject to damage, which is of concern. This is where the PVA came into effect as a binder. As shown in figures 7(a) and (b), the top-view SEM image of the pure GO film shows microstructures of granular-shaped GO, which were formed

during the drying process. Grain boundaries clearly exist and may act as the proton transport channel, but also as the place of structural expansion/contraction when hydration/dehydration occurs. On the other hand, the GO-PVA dielectric shows less sign of grain structure as the GO is surrounded by PVA. AFM images in figure S3 also indicate that PVA incorporation has lowered the surface roughness. Most importantly, the PVA binder has the ability to hold GO together and reduce the expansion/contraction in the microstructure. As a result, the IGZO EDLTs with GO-PVA composite dielectric are more durable than the pure GO ones.

4. Conclusions

In summary, this work introduced a printing deposition method for the fabrication of proton-gated metal-oxide EDLTs. The home-built nozzle jet printing system provided high printing yield and compatibility with a viscous ink containing high density of 2D micro sheets, which might clog the nozzle of normal piezoelectric injection printers. Nozzle jet printing was proved to be a suitable printing method for printing thick dielectric films with viscous inks that are often
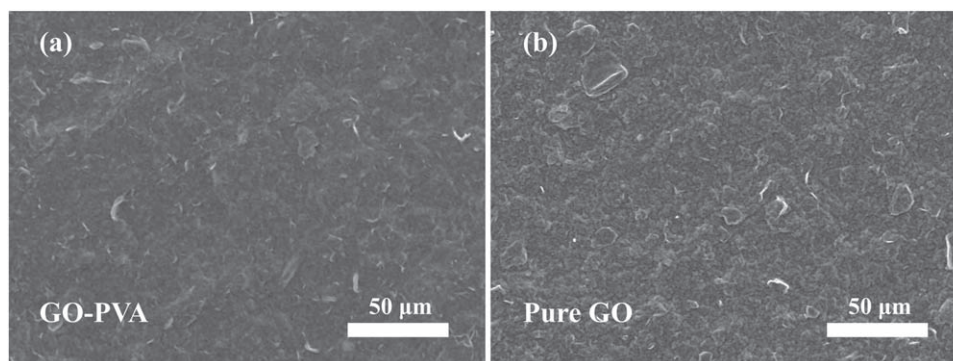
Figure 7. (a) Top-view SEM image of GO-PVA dielectric. (b) Top-view SEM image of pure GO dielectric.

used in EDLTs. The GO-PVA composite dielectric showed typical characteristics of ion-based dielectrics. Reasonable on/off ratio and field mobility were obtained from the IGZO EDLTs in a small gate voltage range. The incorporation of PVA into GO to form the GO-PVA composite dielectric dramatically improved the durability of the prepared devices as PVA binder can provide better structural stability for the dielectric film and the device compared with the pure GO.

Acknowledgments

ORCID iDs

Feng Shao https://orcid.org/0000-0003-1860-2838

References

[1] Panzer M J and Frisbie C D 2005 Polymer electrolyte gate dielectric reveals finite windows of high conductivity in organic thin film transistors at high charge carrier densities *J. Am. Chem. Soc.* **127** 6960–1

[2] Herlogsson L, Crispin X, Robinson N D, Sandberg M, Hagel O J, Gustafsson G and Berggren M 2007 Low-voltage polymer field-effect transistors gated via a proton conductor *Adv. Mater.* **19** 97–101

[3] Takeya J, Yamada K, Hara K, Shigeto K, Tsukagoshi K, Ikehata S and Aoyagi Y 2006 High-density electrostatic carrier doping in organic single-crystal transistors with polymer gel electrolyte *Appl. Phys. Lett.* **88** 112102

[4] Du H, Lin X, Xu Z and Chu D 2015 Electric double-layer transistors: a review of recent progress *J. Mater. Sci.* **50** 5641–73

[5] Said E, Larsson O, Berggren M and Crispin X 2008 Effects of the ionic currents in electrolyte-gated organic field-effect transistors *Adv. Funct. Mater.* **18** 3529–36

[6] Yuan H, Shimotani H, Tsukazaki A, Ohtomo A, Kawasaki M and Iwasa Y 2009 High-density carrier accumulation in ZnO field-effect transistors gated by electric double layers of ionic liquids *Adv. Funct. Mater.* **19** 1046–53

[7] Liu N, Zhu L Q, Feng P, Wan C J, Liu Y H, Shi Y and Wan Q 2015 Flexible sensory platform based on oxide-based neuromorphic transistors *Sci. Rep.* **5** 18082

[8] Zhu L Q, Wan C J, Guo L Q, Shi Y and Wan Q 2014 Artificial synapse network on inorganic proton conductor for neuromorphic systems *Nat. Commun.* **5** 3158

[9] Liu Y H, Zhu L Q, Feng P, Shi Y and Wan Q 2015 Freestanding artificial synapses based on laterally proton-coupled transistors on chitosan membranes *Adv. Mater.* **27** 5599–604

[10] Shao F, Feng P, Wan C, Wan X, Yang Y, Shi Y and Wan Q 2017 Multifunctional logic demonstrated in a flexible multigate oxide-based electric-double-layer transistor on paper substrate *Adv. Electron. Mater.* **3** 1600509

[11] He P and Derby B 2017 Inkjet printing ultra-large graphene oxide flakes *2D Mater.* **4** 021021

[12] Secor E B and Hersam M C 2015 Emerging carbon and post-carbon nanomaterial inks for printed electronics *J. Phys. Chem. Lett.* **6** 620–6

[13] He P, Brent J R, Ding H, Yang J, Lewis D J, O'Brien P and Derby B 2018 Fully printed high performance humidity sensors based on two-dimensional materials *Nanoscale* **10** 5599–606

[14] Yang J-W *et al* 2018 Printable graphene oxide micropatterns for a bio-subretinal chip *Adv. Healthcare Mater.* **7** 1800365

[15] Cukierman S 2006 Et tu, Grotthuss! and other unfinished stories *BBA—Bioenerg.* **1757** 876–85

[16] Karim M R *et al* 2013 Graphene oxide nanosheet with high proton conductivity *JACS* **135** 8097–100

[17] Gao W *et al* 2014 Ozonated graphene oxide film as a proton-exchange membrane *Angew. Chem. Int. Ed.* **53** 3588–93

[18] Gao W *et al* 2011 Direct laser writing of micro-supercapacitors on hydrated graphite oxide films *Nat. Nanotechnol.* **6** 496

[19] Kumar R, Mamlouk M and Scott K 2011 A graphite oxide paper polymer electrolyte for direct methanol fuel cells *Int. J. Electrochem.* **2011** 7

[20] Wan C J, Zhu L Q, Liu Y H, Feng P, Liu Z P, Cao H L, Xiao P, Shi Y and Wan Q 2016 Proton-conducting graphene oxide-coupled neuron transistors for brain-inspired cognitive systems *Adv. Mater.* **28** 3557–63

[21] Ravikumar and Scott K 2012 Freestanding sulfonated graphene oxide paper: a new polymer electrolyte for polymer electrolyte fuel cells *Chem. Commun.* **48** 5584–6

[22] Yoon D G, Kang M, Kim J B and Kang K-T 2018 Nozzle printed-PEDOT:PSS for organic light emitting diodes with various dilution rates of ethanol *Appl. Sci.* **8** 203

[23] Bhat K S, Nakate U T, Yoo J-Y, Wang Y, Mahmoudi T and Hahn Y-B 2019 Nozzle-jet-printed silver/graphene composite-based field-effect transistor sensor for phosphate ion detection *ACS Omega* **4** 8373–80

[24] Wang Y, Khan M Y, Lee S-K, Park Y-K and Hahn Y-B 2016 Parametric study of nozzle-jet printing for directly drawn ZnO field-effect transistors *Sci. Adv. Mater.* **8** 148–55

[25] Shao F and Wan Q 2019 Recent progress on jet printing of oxide-based thin film transistors *J. Phys. D: Appl. Phys.* **52** 143002

[26] Cho J H, Lee J, Xia Y, Kim B, He Y, Renn M J, Lodge T P and Frisbie C D 2008 Printable ion-gel gate dielectrics for low-voltage polymer thin-film transistors on plastic *Nat. Mater.* **7** 900–6

[27] Wu G, Feng P, Wan X, Zhu L, Shi Y and Wan Q 2016 Artificial synaptic devices based on natural chicken albumen coupled electric-double-layer transistors *Sci. Rep.* **6** 23578

[28] Yuan H, Shimotani H, Tsukazaki A, Ohtomo A, Kawasaki M and Iwasa Y 2010 Hydrogenation-induced surface polarity recognition and proton memory behavior at protic-ionic-liquid/oxide electric-double-layer interfaces *J. Am. Chem. Soc.* **132** 6672–8

[29] Ono S, Miwa K, Seki S and Takeya J 2009 A comparative study of organic single-crystal transistors gated with various ionic-liquid electrolytes *Appl. Phys. Lett.* **94** 063301

[30] Larsson O, Said E, Berggren M and Crispin X 2009 Insulator polarization mechanisms in polyelectrolyte-gated organic field-effect transistors *Adv. Funct. Mater.* **19** 3334–41

[31] Sun J, Liu H, Jiang J, Lu A and Wan Q 2010 Low-voltage transparent SnO$_2$ nanowire transistors gated by microporous SiO$_2$ solid-electrolyte with improved polarization response *J. Mater. Chem.* **20** 8010–5

[32] Chai L, Wang T, Zhang L, Wang H, Yang W, Dai S, Meng Y and Li X 2015 A Cu–m-phenylenediamine complex induced route to fabricate poly(m-phenylenediamine)/reduced graphene oxide hydrogel and its adsorption application *Carbon* **81** 748–57

[33] Wu X, Xie Y, Xue C, Chen K, Yang X, Xu L, Qi J and Zhang D 2019 Preparation of PVA-GO composite hydrogel and effect of ionic coordination on its properties *Mater. Res. Express* **6** 075306

[34] Wang C *et al* 2015 Significance of the double-layer capacitor effect in polar rubbery dielectrics and exceptionally stable low-voltage high transconductance organic transistors *Sci. Rep.* **5** 17849